EES Batteries

PAPER

View Article Online
View Journal | View Issue

Cite this: *EES Batteries*, 2025, **1**, 541

Ionic liquid electrolytes for enhancing the performance of lithium–sulfur batteries: a new approach to mitigating polysulfide dissolution and shuttle effects†

Ajit Kumar, *[a] Frederick Nti,[a] Jenny Sun, [a] Mahin Maleki,[a] Steve Rowlands,[b] Paul M. Bayley,[b] Maria Forsyth *[a] and Patrick C. Howlett*[a]

Received 17th January 2025,
Accepted 23rd March 2025

DOI: 10.1039/d5eb00009b

rsc.li/EESBatteries

Despite the potential for a greater energy density than lithium-ion batteries, polysulphide dissolution, the polysulphide shuttle effect, and lithium metal instability impede the commercialization of lithium–sulfur (Li–S) batteries. To overcome these obstacles, this study investigates ionic liquids (ILs) as electrolytes, with a particular emphasis on mixed-anion ILs and high concentrations of lithium salt. As demonstrated by undetectable levels in Raman and UV spectroscopy, our results demonstrate that trimethyl-isobutyl phosphonium (P111i4FSI) with 30 mol% lithium bis(trifluoromethanesulfonyl)imide (LiTFSI) efficiently inhibits polysulphide dissolution. With a specific capacity of 625 mA h g^{-1} (based on sulphur) and a 60% capacity retention after 200 cycles, this electrolyte dramatically enhances Li–S battery performance. These findings show how high-concentration IL electrolytes may stabilise lithium interfaces and reduce polysulfide-related problems, bringing Li–S battery technology closer to real-world uses.

Broader context

Advanced energy storage systems that are scalable, sustainable, and efficient are required due to the pressing worldwide transition towards carbon-neutral technology and renewable energy. Because of the availability of sulphur and its high theoretical energy density, lithium–sulfur (Li–S) batteries have become a viable option for next-generation energy storage. However, problems including the shuttle effect, polysulphide dissolving, and lithium metal instability have prevented them from being widely used since they result in decreased cycle life and capacity fading.

This work advances the field by demonstrating how ionic liquid (IL)-based electrolytes may be utilised to solve these important challenges. These IL electrolytes greatly enhance the electrochemical performance of Li–S batteries by stabilising the lithium metal contact and inhibiting polysulphide dissolution to undetectable levels. The study also identifies a new electrolyte design strategy that strikes a compromise between strong ionic conductivity and chemical stability, providing a workable way to increase battery efficiency and longevity.

By bridging the gap between laboratory-scale developments and the real-world implementation of Li–S batteries, these discoveries enhance energy and environmental science. The enhanced performance made possible by IL electrolytes advances Li–S technology towards commercialisation and aids in the worldwide shift to sustainable energy systems for grid storage, electric car integration, and renewable energy integration.

1. Introduction

Lithium-ion batteries (LIBs) are widely used in various applications. Still, their storage capacity, approximately 300 W h kg^{-1},[1,2] is not sufficient for large-scale systems such as electric vehicles (EVs) and grid storage. One of the most promising alternatives is lithium–sulfur (Li–S) batteries which utilize a sulfur cathode and a lithium metal anode. Due to the high theoretical specific capacity of Sulfur (1672 mA h g^{-1}) and Lithium–metal (3800 mA h g^{-1}) Li–S batteries have the potential to deliver a much higher energy density of up to 2500 W h kg^{-1} with 100% utilization of active materials, which is nearly eight times that of current advanced LIBs, making them a strong candidate for next-generation energy storage systems where light weight is a key performance driver.

In Li–S batteries, the discharge process involves the reduction of sulfur (S_8) to lithium sulfide (Li_2S). This happens through a two-voltage plateau mechanism where intermediate polysulfides (Li_2S_n, $n \geq 3$) are formed and dissolved in the electrolyte before being reduced to insoluble lithium-sulfides

[a]*Institute for Frontier Materials(IFM), Deakin University, Burwood, VIC 3125, Australia. E-mail: ajit.kumar@deakin.edu.au, maria.forsyth@deakin.edu.au, patrick.howlett@deakin.edu.au*

[b]*Li-S Energy, Deakin University, 75 Pigdons Rd, Waurn Ponds, Victoria 3216, Australia*

† Electronic supplementary information (ESI) available. See DOI: https://doi.org/10.1039/d5eb00009b

(Li_2S_2 and Li_2S).[3,4] When the battery is charged, the process is reversed: lithium sulfides are oxidized back into sulfur, again forming polysulfide intermediates during the reaction. This reversible reaction gives Li–S batteries a high energy density capability.

Despite the promise of Li–S batteries, they have not yet been commercialized due to the major challenge of the "polysulfide shuttle" (PS) effect. During cycling, the soluble polysulfides formed at the cathode can dissolve in the electrolyte and travel to the anode, where they can react with the lithium metal anode. This so-called shuttle effect of polysulfides leads to unwanted side reactions, causing the rapid loss of active material, capacity fading, and poor coulombic efficiency. The deposition of insoluble lithium sulfide (Li_2S) at the anode-electrolyte interface further contributes to these issues by forming a barrier that hinders lithium-ion transport.[5,6]

In addition to the polysulfide shuttle effect, lithium deposition at the metal anode remains a significant challenge in lithium–sulfur (Li–S) batteries. In electrolytes containing polysulfides, lithium growth often forms dendritic/mossy structures.[7,8] This results in the anode experiencing volume expansion, which compromises mechanical stability and shortens the battery's cycle life.

Although Li–S batteries hold the promise of achieving high theoretical energy densities, practical issues like unstable anode structures hinder their commercialization. Addressing the challenges of lithium deposition and polysulfide interactions is crucial for overcoming these limitations and fully realizing the commercial viability of Li–S technology.

The choice of electrolyte can play a significant role in the stability of Li–S batteries. The liquid electrolytes commonly investigated in the extensive research of these devices are not realistically practical for large-scale manufacture and deployment due to safety and toxicity-related issues. Furthermore, the electrolytes used in conventional LIBs, such as carbonate-based solvents, are not compatible with Li–S chemistry.[9] Polysulfides react with carbonate solvents, resulting in byproducts that degrade both the electrolyte and the active materials over time.[10]

To avoid these reactions, ether-based solvents such as dioxolane (DOL) and dimethoxyethane (DME) are commonly used in Li–S cells.[11] These solvents are better at stabilizing polysulfides without causing unwanted side reactions. One popular electrolyte formulation is 1 M lithium bis(trifluoromethanesulfonyl)imide (LiTFSI) in a 1 : 1 mixture of DOL and DME, with a 1% weight/weight addition of lithium nitrate ($LiNO_3$). The $LiNO_3$ additive helps passivate the lithium metal anode, preventing the polysulfides from reacting with it.[12] However, this protection is lost once the $LiNO_3$ is consumed, and the polysulfide shuttle effect resumes.[13,14] Furthermore, the volatile and potentially explosive nature of $LiNO_3$.[15,16] presents additional safety concerns, making it challenging to manufacture large-scale Li–S cells with this electrolyte.

Controlling the dissolution of polysulfide intermediates is essential for extending the cycle life of Li–S batteries while maintaining high energy density. Electrolytes with a lower ability to dissolve polysulfides are preferred because they reduce the shuttle effect.[6,17] However, achieving low polysulfide solubility is difficult due to the complex nature of sulfur and lithium polysulfides. Sulfur (S_8) is hydrophobic and only dissolves in non-polar solvents like benzene, while the fully reduced product, Li_2S, is hydrophilic and only dissolves in highly polar solvents like water.[18] The intermediate polysulfides (Li_2S_n) exhibit varying degrees of polarity depending on their chain length, making it hard to design an electrolyte that works well with all forms of polysulfides.

In addition to controlling polysulfide solubility, the electrolyte must be a good solvent for the lithium salt and must be able to form a stable passivation layer on both the anode and cathode; *i.e.* a stable, homogeneous SEI/CEI on the electrodes.

Previous research has explored the use of ionic liquids (ILs) as electrolytes in Li–S batteries. Watanabe's group studied the solubility of sulfur and lithium polysulfides (Li_2S_n, $4 \leq n \leq 8$) in ionic liquids with different anions and found that ILs with bis(trifluoromethanesulfonyl)imide (TFSI) anions were effective in reducing polysulfide dissolution.[19] These TFSI-based ILs showed low sulfur solubility (about 10 mM atomic sulfur), making them suitable candidates for Li–S batteries, with the best results obtained for an electrolyte composition of 0.5 mol kg^{-1} LiTFSI in *N*-methyl-*N*-propylpyrrolidinium bis(trifluoromethane sulfonyl)imide provide discharge capacity of 600 mA h g^{-1} at the 50th cycle. The other IL-based electrolyte systems performed poorly due to high polysulfide solubility, side reactions, and slow mass transport.[20]

In other work, ILs with the smaller fluor sulfonyl imide (FSI) anion did not perform well in Li–S cells;[19,21] despite effectively suppressing polysulfide dissolution, they caused significant capacity loss and high overpotential within the first 10 cycles. This was likely due to excessive decomposition of the FSI anion, resulting in an insulating layer on the sulfur cathode with concomitant charge transfer resistance. As a result, TFSI-based ILs have been considered the most promising for Li–S batteries due to their ability to balance low polysulfide solubility and stable cycling performance.[22]

Several individual challenges need to be addressed to enhance the performance of Li–S batteries and make them commercially viable; these include the control of polysulfide dissolution, the ability to cycle high-capacity lithium anodes without dendrite formation, and discovering an electrolyte that can withstand the highly reactive nature of both the metal Li anode and reactive polysulfide intermediates and form robust, low ionic-resistance passivating layers on both electrodes. The electrolyte is a key component in solving these challenges. Our previous work has shown that high, near-saturation concentrations of LiFSI in various ionic liquids can support high-rate cycling of Li metal anodes as well as high-voltage layered oxide cathodes.[23] We have also shown that certain IL chemistries and compositions exhibit extremely low solubility for intermediate polysulfides (Li_2S_n, $4 \leq n \leq 8$).[24]

In this work, we further show that IL electrolytes based on trimethyl, isobutyl phosphonium [P111i4] [FSI] with the addition of LiTFSI dissolve polysulfides at such low levels that

their concentration in the solution is typically below 1 mM sulfur, or even undetectable using UV-vis and Raman spectroscopy. This ultra-low solubility makes them ideal for suppressing the polysulfide shuttle effect in Li–S cells. Additionally, these electrolytes form a low-impedance passivating layer on both the cathode and anode, further enhancing cell performance by limiting polysulfide dissolution.

This discovery marks a significant advancement in Li–S battery technology. By combining ultra-low polysulfide solubility with stable interface formation, these electrolytes enable a quasi-solid-state sulfur redox process, leading to improved cycle life, and overall better performance for Li–S batteries.

2. Results and discussion

2.1. Cycling performance of Li metal symmetric cell

Symmetric Li|Li cells provide a valuable platform for assessing the reversibility of lithium deposition and stripping processes, effectively simulating anode conditions without interference from insertion cathode materials. In this study, cells were cycled at an elevated temperature of 50 °C to capitalize on the enhanced ionic conductivity of the electrolyte. Fig. 1a presents the cycling performance of a cell containing 30 mol% LiTFSI in a P_{111i4}FSI-based electrolyte, with a high-charge capacity of 4 mA h cm^{-2}, comparable to that used in commercial Li-ion cells, at a current density of 1 mA cm^{-2}. Fig. 1b and c illustrate the voltage-time profiles during initial cycling and after 300 hours of operation, respectively. Notably, even after 300 hours of repeated lithium plating and stripping, the potential profile exhibits remarkable stability, highlighting the electrolyte's ability to maintain electrochemical performance over extended cycling. This stability is indicative of the intrinsic advantages of using an ionic liquid-based electrolyte (IL) in terms of both conductivity and long-term reversibility, making it a strong candidate for advanced Li metal batteries. These findings also demonstrate the robustness of the electrolyte under moderately high-temperature conditions, supporting its potential for improving the longevity and reliability of next-generation Li-metal cells. Fig. S1† presents the temperature-dependent physicochemical properties of P_{111i4}FSI and Li-LiTFSI mixtures. Panel (a) illustrates that the ionic conductivity of the electrolytes decreases with increasing salt concentration. Panel (b) shows that the density of the mixtures increases with higher salt concentrations. Panel (c) depicts a decrease in the lithium diffusion coefficient as salt concentration rises. Lastly, panel (d) reveals that the viscosity of the electrolytes increases with higher salt concentrations.

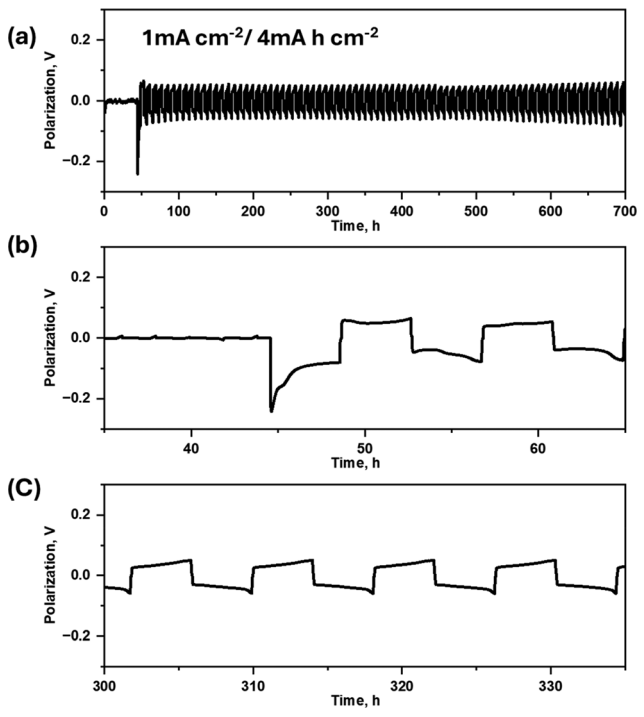

Fig. 1 Li metal symmetric cell cycling: (a) voltage profiles during lithium plating/stripping processes in Li|Li symmetrical cells containing 30 mol% LiTFSI in P_{111i4}FSI electrolytes at current density 1.0 mA cm^{-2} (4 mA h cm^{-2}), at 50 °C (b) and (c) are the zoomed view.

2.2. Polysulfide dissolution test

One of the biggest challenges in lithium–sulfur (Li–S) batteries is the issue of polysulfide dissolution in the electrolyte. This leads to a phenomenon called "polysulfide shuttling", where polysulfides move back and forth between the lithium anode and sulfur cathode. This shuttling reduces the effectiveness of the sulfur-active material and causes the battery capacity to fade quickly. To address this, we conducted a test to check the solubility of lithium polysulfides in a pure ionic liquid (P_{111i4}FSI) and a mixture of P_{111i4}FSI with different concentrations of lithium bis(trifluoromethanesulfonyl)imide (LiTFSI). We used LiTFSI concentrations of 5, 10, 20, 30, 40, 45, and 50 mol%. The test was conducted at 50 °C to observe how lithium polysulfides dissolve in the solutions. Stoichiometric mixtures of elemental sulfur powder and lithium sulfide (Li_2S) were prepared in a 7 : 1 ratio, which serves as the source for lithium polysulfides, particularly those with four or more sulfur atoms (Li_2S_n, where $n \geq 4$). This ratio was chosen to ensure enough sulfur atoms were available to form lithium octasulfide (Li_2S_8), which is known to be the most soluble polysulfide in various types of electrolytes including ionic liquid-based electrolytes.[13,19] After adding a fixed amount of lithium polysulfide precursors (elemental sulfur and Li_2S) to each liquid solution, we monitored the color change over time using a digital camera. This color change was used to track the formation of polysulfides. Fig. 2a shows the color change before and after adding the polysulfide precursors to solutions with 0, 5, 10, and 20 mol% LiTFSI in P_{111i4}FSI. Initially, the liquid solutions were clear and transparent, indicating that all LiTFSI had dissolved without residue. After 1 hour of adding the polysulfide precursors, a noticeable color change occurred. Interestingly, the intensity of the color change decreased as the concentration of LiTFSI increased. The pure ionic liquid (without LiTFSI) turned the darkest red color, while the solution with 20 mol% LiTFSI showed only a

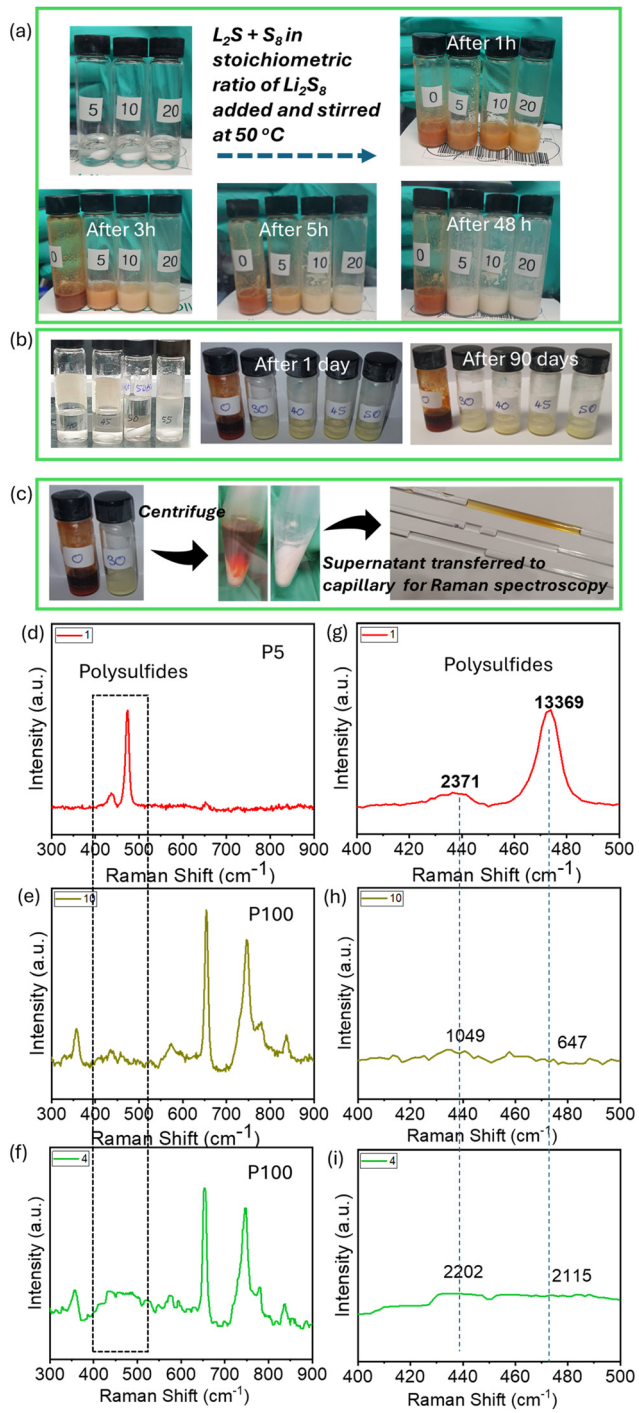

Fig. 2 Polysulfide dissolution test: (a) display of the color change of neat-IL and low-concentration electrolytes (0, 5, 10 and 20 mol% LiTFSI in $P_{111i4}FSI$ IL) after the addition of Li_2S and sulfur powder at 50 °C. (b) Display of the color change of neat-IL and moderate and high-concentration electrolytes (0, 30, 40, 45 and 50 mol% LiTFSI in $P_{111i4}FSI$ IL) before and after the addition of Li_2S and sulfur powder at 50 °C. (c) Steps of sample preparation for Raman-spectroscopy. Raman spectra of (d) Li_2S + S in $P_{111i4}FSI$ IL by utilizing 5% of LAZER power (e) Li_2S + S in 30 mol% LiTFSI in $P_{111i4}FSI$ IL by utilizing 100% of LAZER power (f) 30 mol% LiTFSI in $P_{111i4}FSI$ IL by utilizing 100% of LAZER power. (g, h, and i) are the zoomed view of (d, e, and f) respectively.

light color change. We can link the formation of soluble polysulfides to the observed color change, with less polysulfide formation in solutions with higher LiTFSI concentration, showing that the combination of LiTFSI and $P_{111i4}FSI$ reduces the solubility of lithium polysulfides, with this effect increasing as the LiTFSI concentration rises.

After 3 hours of stirring, the color intensity of all the solutions, except for the pure ionic liquid, decreased. The time it took for the color to disappear was inversely proportional to the LiTFSI concentration. After 48 hours, all solutions became colorless, except for the pure ionic liquid. This color disappearance could be due to the reverse reaction, where polysulfides convert back into elemental sulfur and Li_2S. Even a small amount of polysulfides can degrade battery performance if present in the electrolyte for more than an hour, thus ideally, we want to decrease the concentration to negligible values.

To further ensure that polysulfide formation was fully suppressed in our electrolyte, we further tested solutions with LiTFSI concentrations above 20 mol%. Fig. 2b shows the color changes in solutions with 0, 30, 40, 45, and 50 mol% LiTFSI, both before and after adding Li_2S and elemental sulfur powder at 50 °C. Interestingly, none of these solutions, except for the pure ionic liquid, showed any color change, even after 90 days, suggesting no significant polysulfide dissolution occurred in electrolytes with 30 mol% or more LiTFSI. Raman spectroscopy, known to be a highly sensitive technique for detecting polysulfides, was used to confirm that even trace amounts of polysulfides were not forming in the electrolyte. Polysulfides can be identified by their characteristic Raman peaks in the 400–500 cm^{-1} range, which correspond to the S–S stretch vibration of the polysulfide molecules.[25–27] Fig. 2c illustrates the sample preparation process for this test. We examined two samples: one with pure ionic liquid (neat IL) saturated with lithium polysulfides and another with 30 mol% LiTFSI in $P_{111i4}FSI$, also saturated with lithium polysulfides. To ensure polysulfide formation, we stirred the mixtures of elemental sulfur and Li_2S powder for one week at 50 °C, giving ample time for the polysulfides to form and dissolve. The solutions were then allowed to settle for two days. Heating the mixtures to 50 °C provided the necessary thermal energy to promote polysulfide formation. Afterward, the mixtures were centrifuged to separate any unreacted sulfur or Li_2S from the liquid part of the solution. The supernatant liquid was transferred into transparent capillary tubes, which were sealed to prevent contamination from moisture and air during the Raman spectroscopy measurements. The Raman spectra for these samples are shown in Fig. 2d–i. For the sample with pure ionic liquid (0 mol% LiTFSI), the Raman spectra showed clear, sharp peaks at 438 and 474 cm^{-1}, corresponding to dissolved lithium polysulfides. These peaks were detected even with a low laser power of 0.85 mW, which indicates a large quantity of dissolved polysulfides in the solution. In contrast, the Raman spectra of the colorless solution with 30 mol% LiTFSI did not show any detectable polysulfide peaks, even when illuminated with a much higher laser power of 17 mW (20 times

higher than the power used for the pure ionic liquid sample). This suggests that the amount of dissolved polysulfides in the 30 mol% LiTFSI solution was extremely low or absent. For comparison, we also examined a blank electrolyte containing 30 mol% LiTFSI in $P_{111i4}FSI$ without any added sulfur or Li_2S. The results showed no significant Raman peaks in this blank sample either. These findings indicate that high concentrations of LiTFSI in the $P_{111i4}FSI$ ionic liquid (30 mol% and above) effectively suppress the dissolution of lithium polysulfides. We can thus conclude that electrolytes based on LiTFSI in $P_{111i4}FSI$ with 30 mol% or more LiTFSI significantly reduce polysulfide formation and dissolution which should lead to the improvement of the overall stability and performance of Li–S batteries.

2.3. Quantification of polysulfides concentration

While the study above qualitatively indicated suppression of polysulfides in the IL electrolytes, we also conducted a series of experiments using Raman and UV spectroscopy in an attempt to quantify the concentration of polysulfides in different electrolyte solutions. Specifically, we focused on two types of samples: one containing neat ionic liquid ($P_{111i4}FSI$) with various concentrations of lithium polysulfides, and the other containing 30 mol% LiTFSI in $P_{111i4}FSI$, also saturated with lithium polysulfides. The Raman spectra for the neat ionic liquid ($P_{111i4}FSI$) containing lithium polysulfides at concentrations of 2.5 mM and 1.25 mM sulfur are displayed in Fig. 3a and b, respectively. To provide a clearer view, the zoomed-in versions are shown in Fig. 3e and f. Given the high sensitivity of the Raman spectroscopy technique, we were able to detect clear peaks in both samples. This confirms that the Renishaw inVia Visible Raman Microscope, equipped with a 633 nm laser, operating at 17 mW power and 20x magnification, is capable of detecting even very small amounts of lithium polysulfide species in the $P_{111i4}FSI$ ionic liquid.

We then analyzed the Raman spectra of the mixed anion electrolyte, which contained 30 mol% LiTFSI in $P_{111i4}FSI$ and was saturated with lithium polysulfides. These results, along with the spectra for the blank electrolyte (without any lithium polysulfides), are presented in Fig. 3c and d, with zoomed-in views in Fig. 3g and h. After comparing the spectra from Fig. 3f, g, and h, we can conclude that the solubility of lithium polysulfides in the 30 mol% LiTFSI in $P_{111i4}FSI$ electrolyte is extremely low such that even the highly sensitive Raman spectroscopy could not detect any species when operating at full laser power (100%). In addition to Raman spectroscopy, we also used UV spectroscopy (UV-2600, SHIMADZU) to further analyze the solubility of polysulfides in both the neat $P_{111i4}FSI$ and the 30 mol% LiTFSI/$P_{111i4}FSI$ mixture. Fig. 3i shows the UV absorption spectra for these solutions. While UV-VIS spectra are generally challenging for determining the exact composition of polysulfide species, previous research has identified the absorption bands for various polysulfides: 490–500 nm for S_8^{2-}, 450–470 nm for S_6^{2-}, and around 420 nm for S_4^{2-}.[20]

In Fig. 3i the black-colored graph represents the UV spectrum for the 30 mol% LiTFSI in $P_{111i4}FSI$ solution, saturated

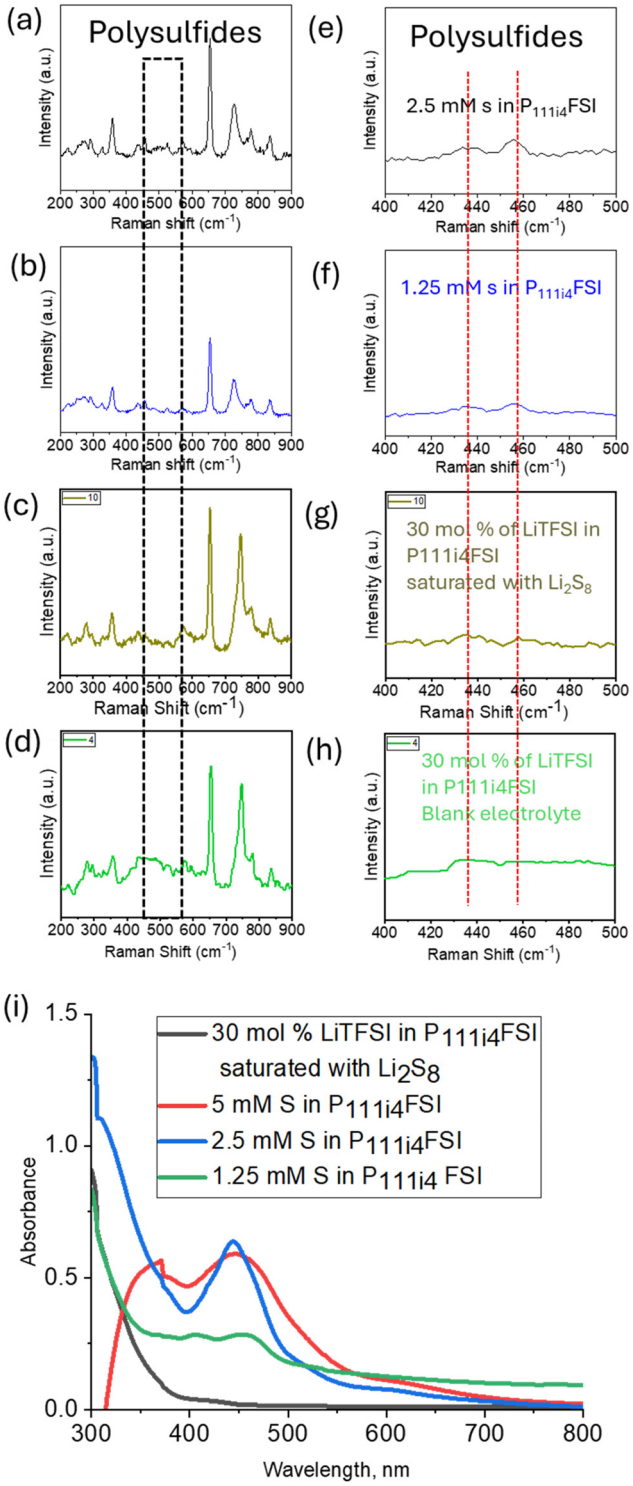

Fig. 3 Quantification of polysulfides concentration: Raman spectra: (a) 2.5 and (b) 1.25 mM S (sulfur) in $P_{111i4}FSI$ IL, (c) 30 mol% LiTFSI in $P_{111i4}FSI$ IL saturated with lithium-polysulfides, (d) 30 mol% LiTFSI in $P_{111i4}FSI$ IL by utilizing 100% of LAZER power. (e, f, g and h) are the zoomed view of (a, b, c, and d) respectively. (i) UV-spectroscopy of 1.25 (green), 2.50 (blue) 5.00 (red) mM S (sulfur) in $P_{111i4}FSI$ IL, and 30 mol% LiTFSI in $P_{111i4}FSI$ IL electrolyte saturated with lithium-polysulfides (black).

with Li_2S_8 and other lithium polysulfides (Li_2S_n, $n \geq 4$). This graph shows nearly zero absorbance above 400 nm, indicating that none of these polysulfide species (S_8^{2-}, S_6^{2-}, S_4^{2-}) were detectable in the solution at levels measurable by UV spectroscopy. In contrast, the green-colored graph represents the lowest concentration sample (1.25 mM sulfur in $P_{111i4}FSI$ without any Li salt), which shows significant UV absorption, confirming the presence of detectable amounts of sulfur. This comparison suggests that the concentration of sulfur in the 30 mol% LiTFSI in $P_{111i4}FSI$ solution is far lower than 1.25 mM. It is likely below the quantification or detection limits of the UV and Raman spectroscopy methods we used. This finding indicates that the solubility of polysulfides in the 30 mol% LiTFSI electrolyte is extremely low-essentially negligible or close to zero.

Overall, both the Raman and UV spectroscopy results verify the above conclusion that high concentrations of LiTFSI in $P_{111i4}FSI$ greatly suppress the dissolution of lithium polysulfides. Having satisfied ourselves that these mixed anion, high salt concentration LiTFSI in $P_{111i4}FSI$ electrolytes can both support Li metal cycling and suppress the presence of polysulfide, we further investigated these electrolytes in full cell configurations as discussed below.

2.4. Electrochemical performance of Li–S cells

In this study, coin cells were made with a sulfur electrode as the cathode and a thin 50 μm lithium foil as the anode. Initially, the cells were in a charged state with an open circuit potential (OCP) of 3.0 V. The Li–S cell was first fully discharged to complete the reduction process.

Fig. 4a shows how the discharge capacity changes over cycles for Li–S cells using different electrolyte compositions: 10 mol% LiFSI (black), 30 mol% LiFSI (red), 10 mol% LiTFSI (blue), 30 mol% LiTFSI (green), 50 mol% LiFSI (purple), and 50 mol% LiTFSI (yellow) in the $P_{111i4}FSI$ ionic liquid electrolyte at 50 °C. Fig. 4b presents the charge capacity over the cycles, while Fig. 4c illustrates the coulombic efficiency (how well charge is retained) for each cycle. Fig. 4d shows the discharge capacity for the 10th and 20th cycles of these cells, and Fig. 4e highlights the coulombic efficiency for the 1st and 20th cycles. Long-term cycling performance, shown in Fig. 4f, compares discharge–charge capacity over time for cells with 30 mol% LiTFSI, 50 mol% LiFSI, and 50 mol% LiTFSI in $P_{111i4}FSI$ electrolytes. Here the high concentration LiFSI in $P_{111i4}FSI$ is used as a comparison since this electrolyte composition has previously been shown to support high-rate, high-capacity cycling.[28] The charge–discharge cycling was conducted within a voltage range of 1.5–2.8 V *vs.* Li/Li^+. During discharge, the cells displayed a single voltage plateau at 2.0 V, which likely corresponds to a quasi-solid–solid transition from S_8 to Li_2S_n (Fig. 4g). During the charge cycle, a single plateau at 2.4 V indicates the oxidation of lower-order polysulfides back to elemental sulfur (S_8).[13] Fig. 4h shows the capacity retention after the 20th and 200th cycles for cells with 30 mol% LiTFSI, 50 mol% LiFSI, and 50 mol% LiTFSI in $P_{111i4}FSI$ electrolytes.

Fig. S2† demonstrates that the $P_{111i4}FSI$-based electrolyte with LiFSI salt also significantly enhances the utilization of the cathode active material, resulting in considerably higher charge and discharge capacities compared to traditional solvent-based electrolytes. As illustrated in Fig. S3,† increasing the LiFSI salt concentration to 30 mol% within the $P_{111i4}FSI$ electrolyte improves cathode utilization more effectively than a lower concentration of 10 mol%. Similarly, Fig. S4† shows that the $P_{111i4}FSI$-based electrolyte with LiTFSI salt markedly boosts cathode active material utilization, leading to higher charge and discharge capacities compared to conventional electrolytes. As depicted in Fig. S5,† increasing the LiTFSI salt content to 30 mol% in the $P_{111i4}FSI$ electrolyte enhances cathode utilization more than a 10 mol% concentration of the same salt. This is consistent with the hypothesis that highly concentrated IL electrolytes can reduce polysulfide dissolution in the electrolyte.

A wholistic view of the effect of electrolyte composition on Li–S cell performance is presented in Fig. 4. The data shows that a concentration of LiTFSI salt (30 mol%) in the mixed FSI/TFSI anion electrolyte and 50 mol% of LiFSI in single anion leads to better cathode utilization. In contrast, lower salt concentrations (10 mol% in both LiTFSI and LiFSI) and 30 mol% LiFSI result in a lower capacity. The 30 mol% mixed-anion electrolyte cell delivered a discharge capacity of ~1050 mA h g^{-1} in the first cycle and ~740 mA h g^{-1} in the 20th cycle, while the 50 mol% single-FSI-anion electrolyte cell showed ~1030 mA h g^{-1} initially and ~730 mA h g^{-1} after 20 cycles. This demonstrates that similar electrochemical performance can be attained at a lower total salt concentration through the use of a mixed-anion approach. These results highlight how mixed-anion ionic liquid electrolytes can minimize polysulfide dissolution, promote stable and conductive electrode interfaces, and support sustained battery performance with reduced salt content. This indicates that not only a higher lithium salt concentration but also using the mixed TFSI/FSI anions at lower overall Li salt concentration in these IL electrolytes further reduces polysulfide dissolution and appears to support the formation of more stable and conductive electrode interfaces (as will be discussed later). This leads to lower cell polarization, better utilization of the cathode, and more sustained capacity over time.

2.5. Voltage profile and reaction mechanism

The voltage *versus* capacity profile of lithium–sulfur (Li–S) cells shows two distinct discharge plateaus, which are closely linked to the sulfur electrode's reaction mechanism.[5,6] The first plateau, at 2.3 V, represents the reduction of sulfur (S_8) to soluble polysulfides (Li_2S_n, $n \geq 4$). The second plateau, at about 2.1 V, represents the further reduction to insoluble lithium sulfide (Li_2S). These two voltage plateaus highlight key electrochemical processes that affect the cell efficiency and capacity.

Fig. 5a shows the typical discharge curve of Li–S cells in standard electrolytes, with two plateaus at 2.3 V and 2.1 V. The first plateau, at 2.3 V, is due to the formation of higher-order

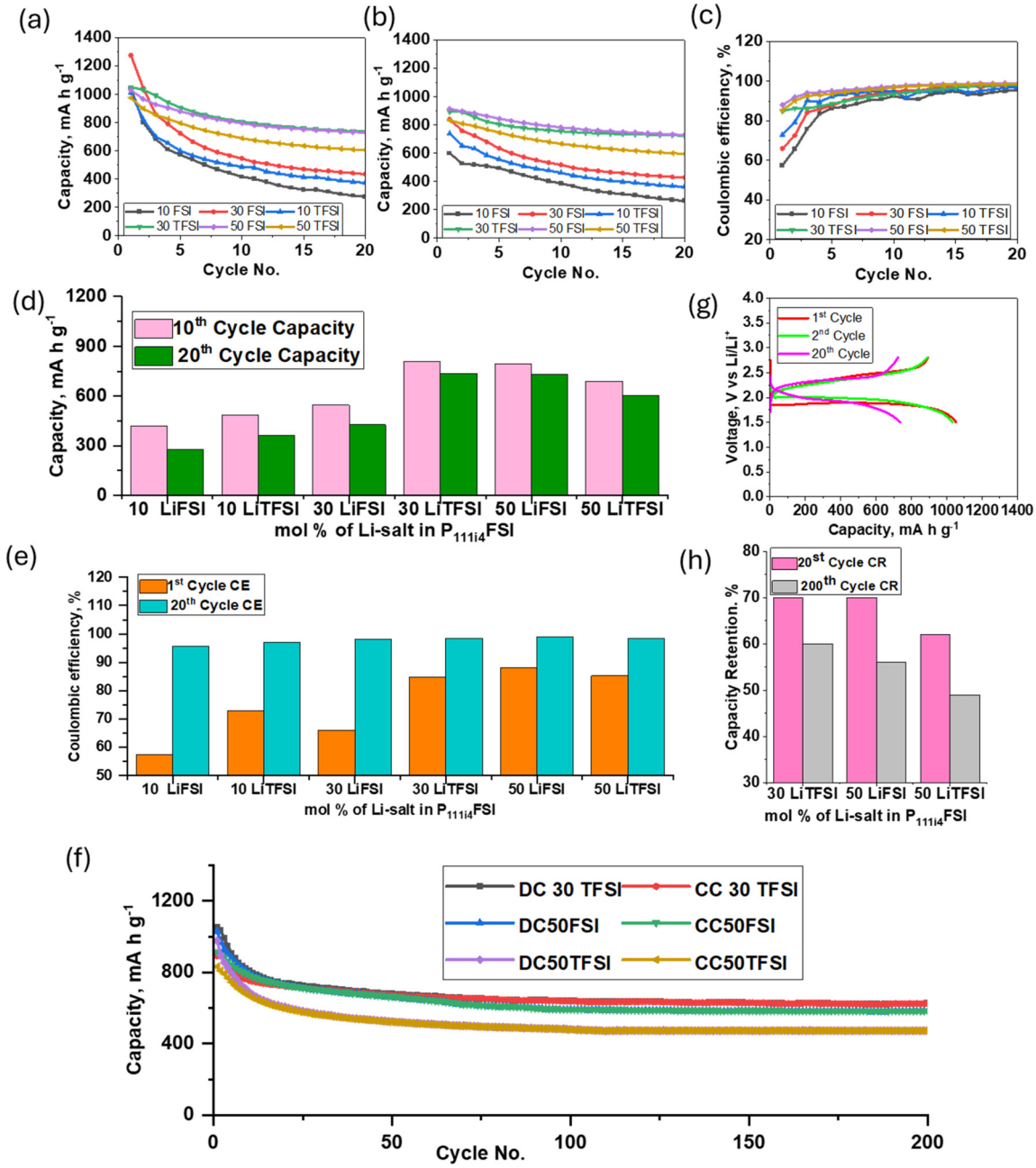

Fig. 4 Electrochemical performance of Li–S cells evaluated at 50 °C with a current density of 167.2 mA g^{-1} for different anion and Li concentration ratios: (a) discharge capacity *versus* cycle number, (b) charge capacity *versus* cycle number, and (c) coulombic efficiency of Li–S cell in 10 mol% LiFSI (black), 30 mol% LiFSI (red), 10 mol% LiTFSI (blue), 30 mol% LiTFSI (green), 50 mol% LiFSI (purple) and 50 mol% LiTFSI (yellow) in $P_{111i4}FSI$ IL-electrolyte at 50 °C. (d) 10^{th} and 20^{th} cycle capacity and (e) 1^{st} and 20^{th} cycle coulombic efficiency for different anion and Li concentration ratios. (f) Long-term cycling (discharge–charge capacity *versus* cycle number) of 30 mol% LiTFSI, 50 mol% LiFSI and 50 mol% LiTFSI in P111i4FSI IL-electrolytes cell. (g) Voltage *versus* charge–discharge capacity profiles of the Li–S cell comprising 30 mol% LiTFSI in P_{111i4} FSI IL-electrolyte. (h) 20^{th} and 200^{th} cycle capacity retention of 30 mol% LiTFSI, 50 mol% LiFSI and 50 mol% LiTFSI in P111i4FSI IL-electrolytes cell.

polysulfide intermediates (Li_2S_n, $n \geq 4$), which dissolve in the electrolyte.[3] The second plateau, at 2.1 V, corresponds to the formation of lower-order sulfides (Li_2S_n, $1 \leq n \leq 2$), which are insoluble.[19] A schematic of possible polysulfide intermediates formed during the lithiation and discharge process is shown in Fig. 5b. This schematic helps compare voltage profiles in different electrolyte systems. Fig. 5c shows the discharge curve of Li–S cells using the new electrolyte studied in this work (30 mol% LiTFSI in $P_{111i4}FSI$), which has a single voltage plateau at 2.0 V. This system follows the quasi-solid-state sulfur reduction, without the formation of higher-order electrolyte soluble polysulfides. The initial discharge capacity of

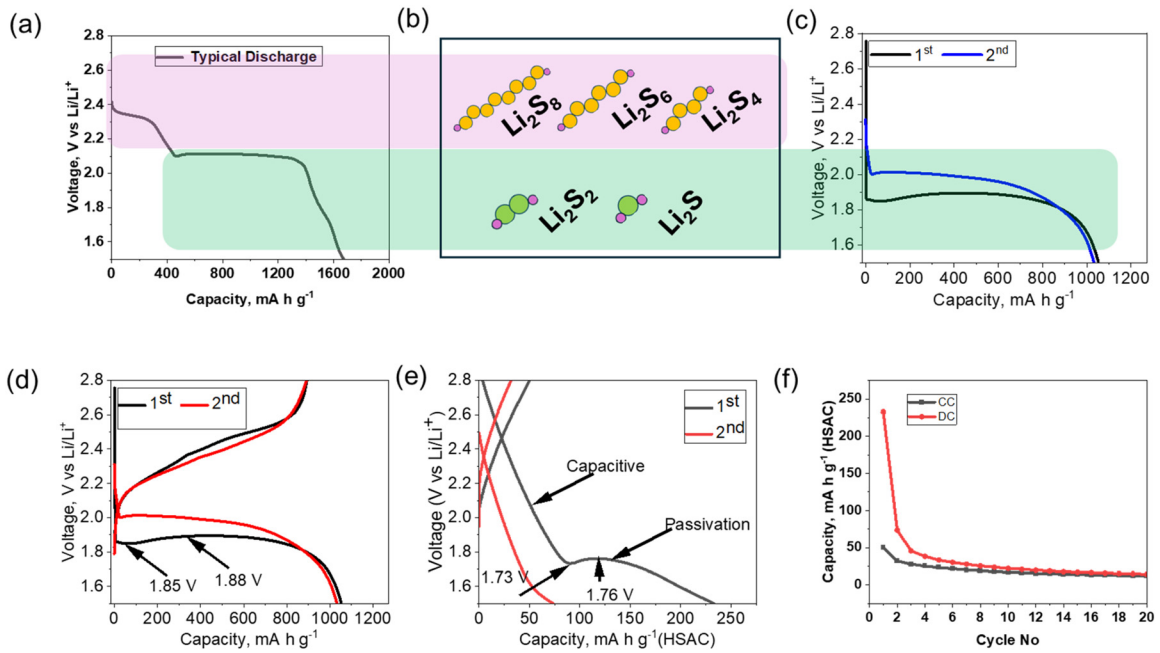

Fig. 5 Voltage profile and reaction mechanism: (a) a typical discharge voltage profile of Li–S cell in 1 M LiTFSI and 0.2 M $LiNO_3$ in 1 : 1 DME : DOL, conventional electrolyte with 100% sulfur utilization. (b) Schematic of possible lithium-polysulfide intermediates. (c) 1st and 2nd discharge voltage profile of Li–S@HSAC cell in IL-electrolyte 30 mol% LiTFSI in $P_{111i4}FSI$. (d) Initial two-cycle discharge–charge voltage profile of Li–S@HSAC cell in IL-electrolyte 30 mol% LiTFSI in $P_{111i4}FSI$. (e) Initial two-cycle discharge–charge voltage profile of Li-HSAC cell in IL-electrolyte 30 mol% LiTFSI in $P_{111i4}FSI$. (f) Discharge–charge/lithiation–delithiation capacity *versus* cycle number of Li-HSAC cell in IL-electrolyte 30 mol% LiTFSI in $P_{111i4}FSI$.

the sulfur electrode is 1050 mA h g^{-1}, around 63% of the sulfur's theoretical capacity.

Fig. 5d shows the discharge–charge curve of Li–S cells using this new electrolyte. The first charge capacity of the sulfur electrode is 890 mA h g^{-1}, which is 60 mA h g^{-1} less than the first discharge capacity. This loss in capacity could be due to irreversible electrolyte decomposition that passivates the sulfur electrode. There is a noticeable difference between the voltage profiles of the first and second discharge cycles. In the first cycle, the discharge voltage plateau at 50% depth of discharge (DOD) is 1.89 V, but this increases to 1.97 V in the second cycle. Similarly, the charge voltage plateau at 50% depth of charge (DOC) decreases from 2.42 V in the first cycle to 2.37 V in the second cycle. These changes in the discharge and charge voltage plateaus may be due to the sulfur electrode–electrolyte interface becoming less resistant.

During the first lithiation, the voltage drops from the open-circuit voltage (OCV) to 1.85 V and then gradually rises to 1.88 V. To separate the effects of electrode passivation from sulfur lithiation, a control cell was made using an electrode of the same composition (HSAC, C65, and CMC) but without sulfur. This control cell, with a lithium metal anode, was cycled at a constant current within the same potential window (1.5 to 2.8 V) using the same 30 mol% LiTFSI in $P_{111i4}FSI$ electrolyte. Fig. 5e shows the discharge–charge curve of the Li-HSAC cells. The initial charge capacity is 50 mA h g^{-1}, mostly capacitive, which is 180 mA h g^{-1} less than its first discharge capacity. This loss in capacity is likely due to irreversible electrolyte breakdown that passivates the HSAC electrode. During the first lithiation, a voltage plateau at 1.76 V indicates electrolyte breakdown. The voltage drops from OCV to 1.73 V and then gradually rises to 1.76 V, possibly due to a decrease in resistance at the electrode–electrolyte interface. Finally, Fig. 5f shows the discharge–charge capacity of Li-HSAC cells over several cycles. After the first few cycles, passivation ends, and only capacitive storage remains.

2.6. Cell impedance/EIS analysis of Li–S cell

We conducted an impedance analysis of lithium–sulfur (Li–S) cells using Electrochemical Impedance Spectroscopy (EIS) to study the interface between the sulfur electrode and the electrolyte. The results are presented in Fig. 6, which compares Nyquist plots from Li–S cells containing the $[P_{111i4}][FSI]$ electrolyte with different lithium salt concentrations. Specifically, the cells tested had 30 mol% LiTFSI (Fig. 6a) and 50 mol% LiFSI (Fig. 6c) in the $[P_{111i4}][FSI]$ IL. Additionally, Fig. 6b and d are zoomed-in views of these respective plots to provide more detail. After the first lithiation of the sulfur electrode, we observed a significant drop in cell resistance. This reduction in resistance is believed to be a result of the modification of the interface between the sulfur electrode and the electrolyte. Specifically, this change is likely due to the formation of a low-resistance, stable solid electrolyte interphase (SEI) facilitated by electrolyte decomposition. During the initial cycle, electrochemical reactions reduce components of the electrolyte (most likely the FSI and/or TFSI anion), leading to the creation of

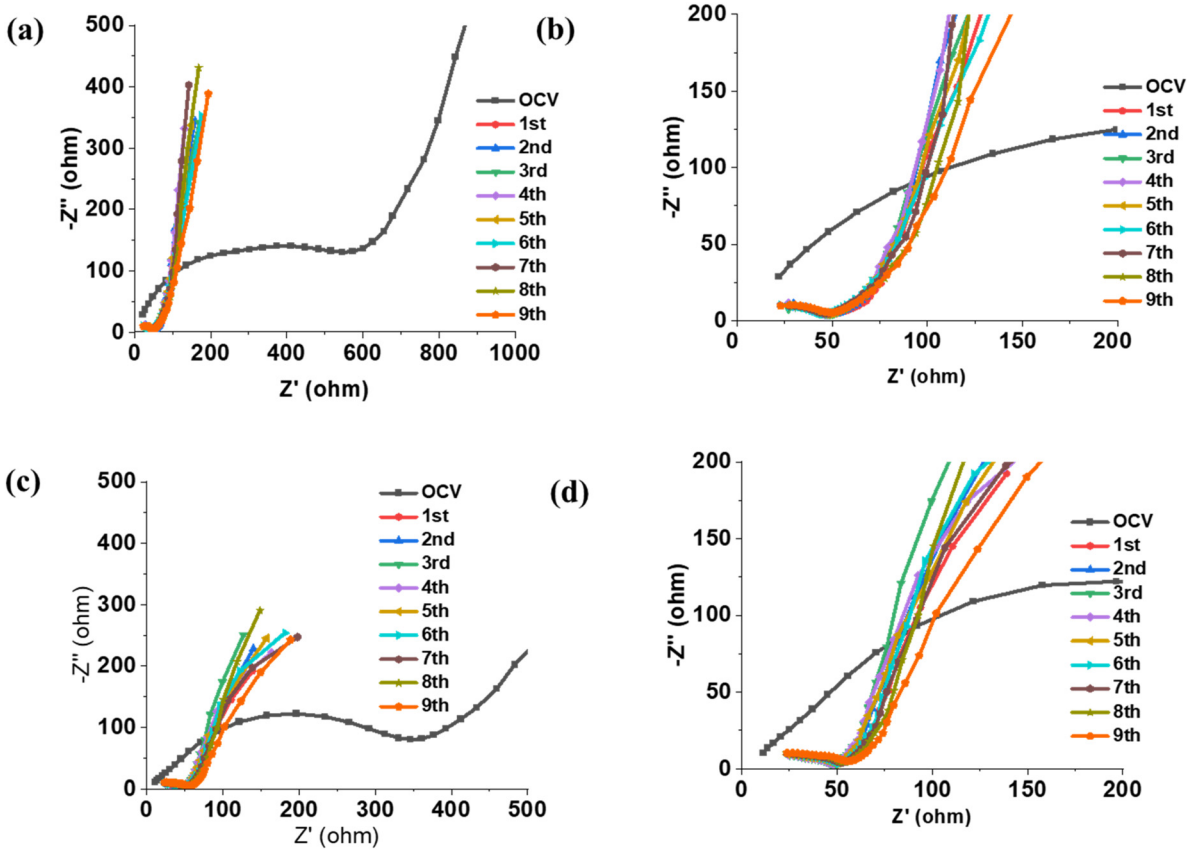

Fig. 6 Electrochemical impedance spectroscopy of LiS cell (15 wt% CMC, 21 wt% HSAC, 14 wt% C65 and 50 wt% S) at OCV and after lithiation in (a) 30 mol% LiTFSI in $P_{111i4}FSI$ IL and (c) 50 mol% LiFSI in $P_{111i4}FSI$ FSI IL electrolyte. (b, and d) are the zoomed view of (a, and c) respectively.

this stable interface interphase. Once the sulfur electrodes are lithiated, the resistance of the cell stabilizes. Fig. 6a and c show the cell resistance up to the 9th cycle. Notably, there is no significant change in cell resistance during cycling. The ability of the electrolyte, especially in the mixed anion system, to maintain a stable sulfur electrode–electrolyte interface suggests that very few, if any, parasitic reactions continue to occur at the electrode. The formation of this stable SEI is a crucial factor in the performance of Li–S cells, as it minimizes unwanted reactions that can degrade the battery over time. These findings highlight the effectiveness of the electrolyte in supporting the long-term operation of Li–S batteries by maintaining a low-resistance, stable interface between the sulfur electrode and electrolyte.

The electrochemical impedance spectroscopy (EIS) analysis of Li–S cells is modelled using an equivalent circuit Fig. 7(a), which includes different resistances and constant phase element (CPE) representing key cell processes. R_{el} represents the bulk resistance of the ionic liquid electrolyte, $R_{SEI,Li}$ corresponds to the resistance of the solid-electrolyte interphase (SEI) at the lithium anode, and $R_{SEI,S}$ represents SEI resistance at the sulfur cathode. The charge transfer resistance at the sulfur electrode ($R_{CT,S}$) reflects the kinetics of the S redox reactions. A constant phase element for diffusion (CPE_{diff}) models lithium-ion diffusion limitations at low frequencies, highlighting mass transport effects in the electrolyte and electrode structure.

Observing the electrochemical behaviour with 30 mol% LiTFSI in $P_{111i4}FSI$ at open circuit voltage (OCV) Fig. 7(b), the charge transfer resistance at the sulfur electrode ($R_{CT,S}$), prior to lithiation, is 585 Ω, indicating an impediment to the electrochemical reactions which would lead to slow reaction kinetics. The charge transfer resistance at the sulfur electrode ($R_{CT,S}$) decreases from 585 Ω at OCV to 96 Ω post-lithiation as shown in Fig. 7(c). After lithiation, $R_{SEI,S}$ is 7.7 Ω, the SEI resistance at the lithium electrode ($R_{SEI,Li}$) decreases from 149.7 Ω at OCV to 20.25 Ω after lithium stripping, signifying the modification of a passivation layer that stabilizes the lithium electrode.

Fig. 7(d) and (e) display the EIS spectra for 50 mol% LiFSI in P111i4FSI electrolyte. A similar trend is observed but with lower resistance values. At OCV, $R_{CT,S}$ is 349 Ω which decreases to 46.3 Ω after the first lithiation step. After lithiation, $R_{SEI,S}$ is 7.4 Ω the SEI resistance at the lithium electrode ($R_{SEI,Li}$) decreases from 279 Ω at OCV to 38.4 Ω after lithium stripping, signifying the modification of a passivation layer that stabilizes the lithium electrode. Both electrolytes show a significant reduction in charge transfer resistance ($R_{CT,S}$) after lithiation as a result of favorable SEI formation at the sulfur electrode.

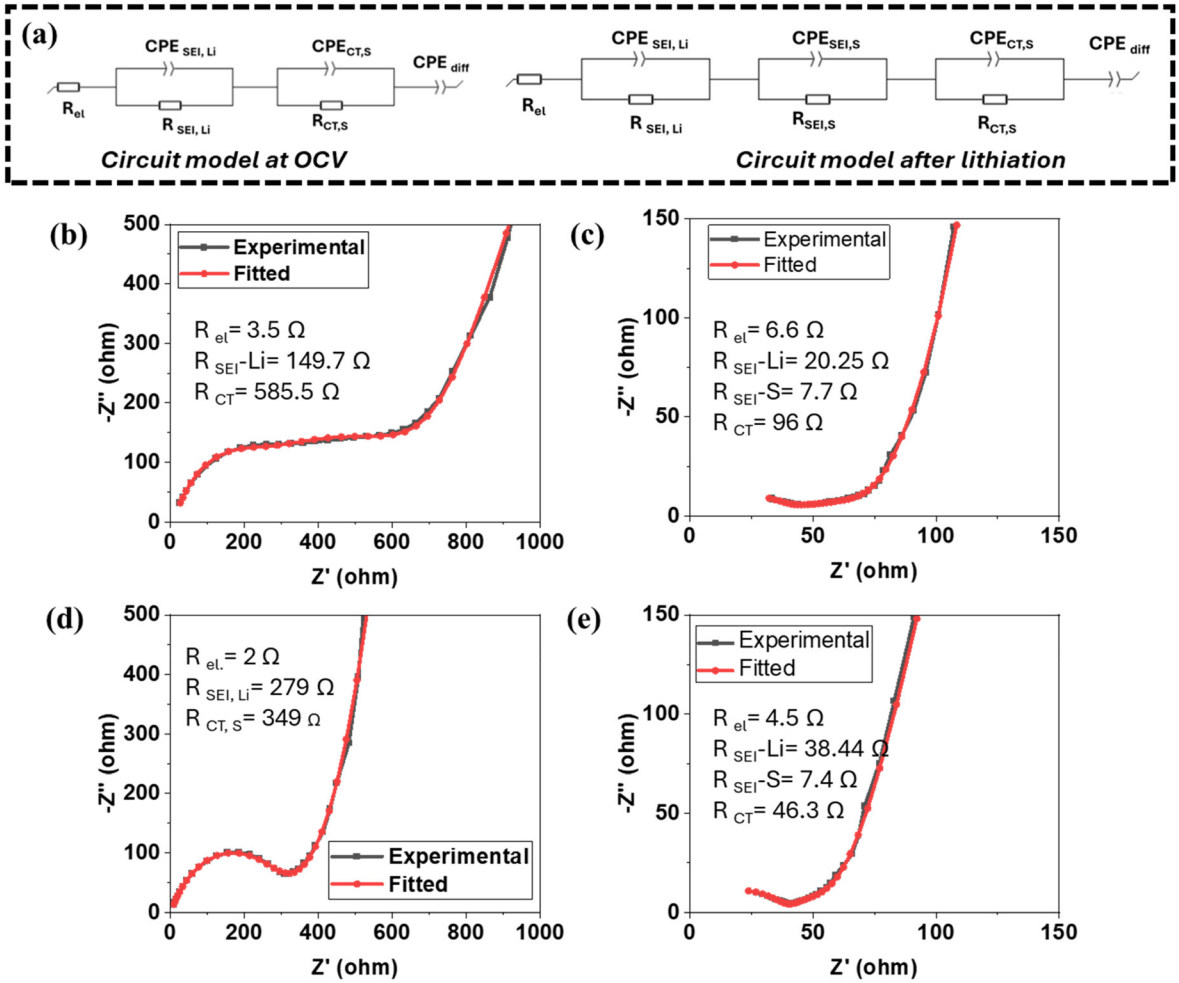

Fig. 7 (a) Equivalent electrical circuit model used for fitting the *in situ* electrochemical impedance spectroscopy (EIS) data. EIS of the Li–S cell (15 wt% CMC, 21 wt% HSAC, 14 wt% C65 and 50 wt% S) in 30 mol% LiTFSI in $P_{111i4}FSI$ IL (b) at OCV and (c) after lithiation, with experimental data (black) and fitted data (red). Electrochemical Impedance spectroscopy of Li–S cell (same electrode composition) (d) at OCV and (e) after lithiation, experimental (black) and fitted (red) in 50 mol% LiFSI in $P_{111i4}FSI$ IL.

2.7. Cell polarization/overvoltage analysis of Li–S cell

To better understand how a stable sulfur electrode–electrolyte interface affects performance, we analyzed the polarization and overvoltage of a lithium–sulfur (Li–S) cell. This was done by studying the relationship between voltage and capacity during cycling. Fig. 8 shows the results of this analysis, where we examined cell polarization during galvanostatic cycling between the 5^{th} and 15^{th} cycles. The cell used a microporous carbon–sulfur cathode with a sulfur loading of 2 mg cm^{-2} and a C-rate of 1/10 (1 C = 1672 mA h g^{-1}). The electrolyte, in this case, was the mixed anion system, containing 30 mol% LiTFSI in $[P_{111i4}][FSI]$.

The difference in voltage between the charge and discharge cycles of the cell, referred to as polarization, is a direct indicator of the stability of the sulfur electrode–electrolyte interface. In general, higher polarization reflects greater cell resistance. A high-resistance interface leads to a more polarized cell, resulting in a large overpotential. This is undesirable, as it decreases the efficiency of the battery. In Fig. 8a, the voltage *vs.* real capacity graph shows the cell performance during cycling. The capacity fade observed could be due to several factors related to the sulfur electrodes. To better understand how polarization evolves during cycling, we normalized the charge and discharge capacity and display the voltage *vs.* depth of discharge–charge capacity, which is shown in Fig. 8b. This normalized graph provides a clearer picture of the cell polarization behavior. The key observation from this analysis is that there was no significant change in polarization during cycling. This indicates that the SEI, formed by the mixed anion ionic liquid electrolyte at the sulfur electrode–electrolyte interface, remained stable throughout the cycling test. Additionally, the combination of a stable SEI and the electrolyte's ability to suppress polysulfide dissolution contributes to the excellent utilization of sulfur and higher discharge capacity. Since the electrolyte has ultralow or negligible solvating power for polysulfides, the cell can maintain its performance over multiple cycles, with minimal loss in capacity.

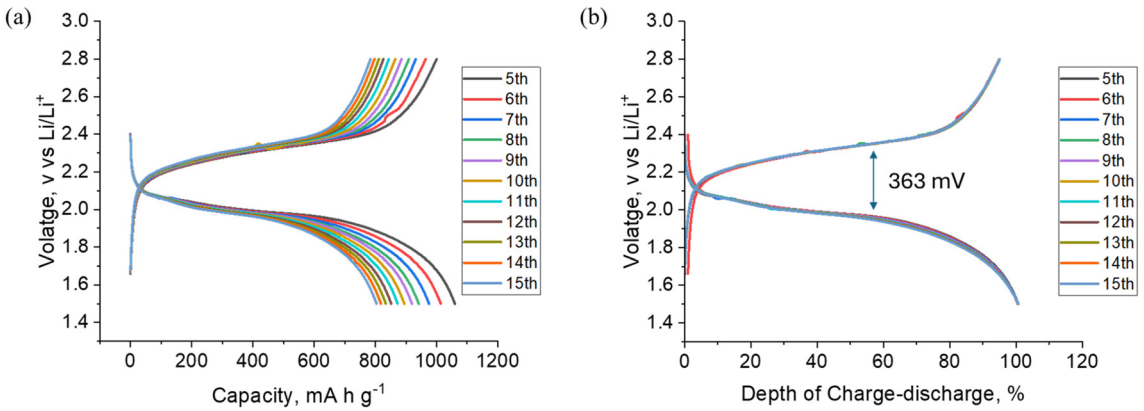

Fig. 8 Overvoltage analysis of Li–S cell: (a) voltage *versus* real charge–discharge capacity and (b) voltage *versus* depth of charge–discharge capacity profiles of the Li–S cell having 30 mol% LiTFSI in $P_{111i4}FSI$ IL-electrolyte.

2.8. Post-cycling analysis of Li–S cell after charge–discharge

We performed a detailed post-cycling analysis of lithium–sulfur (Li–S) cells to examine the behavior of polysulfides during battery operation, particularly their dissolution in the electrolyte. Using UV spectroscopy, we aimed to detect and quantify the polysulfides that form during cycling and potentially become trapped in the separator. Polysulfides, which are intermediates in the sulfur reduction process, can dissolve into the electrolyte, leading to the well-known shuttle effect, which reduces battery performance. Fig. 9a shows an optical image of the cycled lithium anode and sulfur cathode, both of which were covered by the separator. Interestingly, the separator in Fig. 9b, showed no noticeable change in color after cycling, which is often used as an indicator of polysulfide presence. A color change typically suggests polysulfides have diffused into the separator. However, in this case, the lack of visible discoloration indicates that the separator did not trap any detectable amount of polysulfides. Additionally, the surface of the lithium anode appeared shiny and clean, with no visible

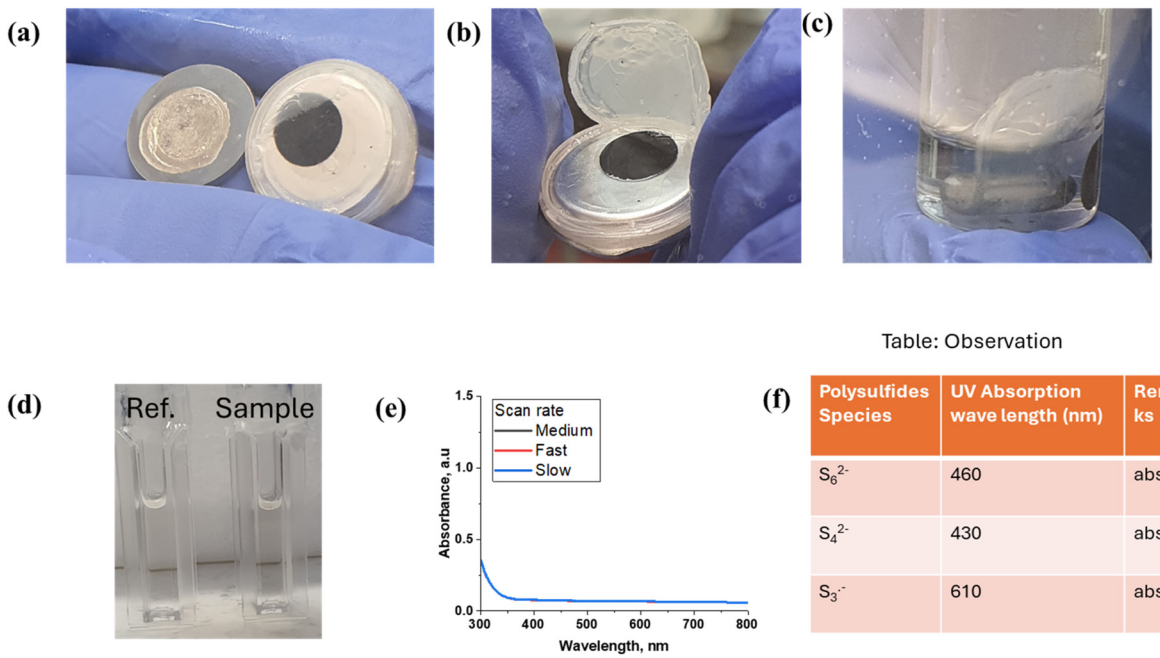

Polysulfides Species	UV Absorption wave length (nm)	Remarks
S_6^{2-}	460	absent
S_4^{2-}	430	absent
$S_3^{\cdot-}$	610	absent

Fig. 9 Post-mortem analyses of LiS cell (15 wt% CMC, 21 wt% HSAC, 14 wt% C65 and 50 wt% S) after 20 cycles in 30 mol% LiTFSI in $P_{111i4}FSI$ IL-electrolyte. (a) An optical image of cycled Li-anode and S-cathode covered with separator. (b) Uncovered S-cathode and separator. (c) S-cathode and separator washed in blank electrolyte 30 mol% LiTFSI in $P_{111i4}FSI$ IL-electrolyte. (d) Optical images of UV-samples blank electrolyte(reference)in left, and electrolyte in which S-cathode and separator washed in the right. (e) UV-spectroscopy of electrolyte in which S-cathode and separator washed, at different scan rates. (f) Table of the expected UV absorption wavelength for different polysulfide species and remarks based on this work's results.

deposits of lithium sulfide (Li_2S). This is significant because the deposition of Li_2S on the anode is one of the major factors contributing to battery performance degradation.

In Fig. 9c, the separator from the cycled cell was washed in neat-IL ($P_{111i4}FSI$) to transfer any polysulfides that may have been trapped in the separator into the ionic liquid solution. This solution was then placed in a sample container for UV spectroscopy analysis to determine the presence of polysulfides. Fig. 9d shows the UV spectra obtained from this analysis. As shown in Fig. 9e, the absorption spectrum displayed nearly zero absorbance above 400 nm. This suggests that none of the higher-order polysulfide species (such as S_8^{2-}, S_6^{2-}, and S_4^{2-}) were present in detectable amounts in the solution. The results from this analysis indicate that the polysulfide concentration in the electrolyte was extremely low and essentially undetectable within the resolution of the UV spectroscopy. This finding suggests that the cycling process in the tested Li–S cell led to minimal polysulfide dissolution. By limiting polysulfide dissolution, the electrolyte can prevent the shuttle effect, which improves battery efficiency and prolongs its lifespan. The clean appearance of the lithium anode and the lack of significant polysulfide absorption in the UV spectra further confirm that the system effectively suppressed the unwanted side reactions typically seen in Li–S batteries, at least under the conditions utilized here (50 °C for 15 cycles).

Conclusions

This study demonstrates that ionic liquid (IL) electrolytes, particularly those with 30 mol% concentrations of lithium bis(trifluoromethanesulfonyl)imide (LiTFSI) and 50 mol% LiFSI in $P_{111i4}FSI$, offer a significant advancement in electrolyte design for the lithium–sulfur (Li–S) battery technology. The research highlights the critical role of ILs in addressing major challenges faced by Li–S batteries, including polysulfide dissolution and shuttle effects. Our findings reveal that ILs with elevated Li-salt concentrations effectively suppress the solubility of lithium polysulfides, reducing their presence to undetectable levels and mitigating the associated performance degradation. The 30 mol% LiTFSI and 50 mol% LiFSI in $P_{111i4}FSI$ electrolyte stand out as particularly effective, showcasing enhanced cycling stability, higher capacity retention, and improved coulombic efficiency compared to other electrolyte formulations. This improved performance is attributed to the electrolyte's ability to form a stable passivating layer (SEI) and limit polysulfide dissolution, thus reducing capacity fade and extending battery life. In summary, the use of 30 mol% LiTFSI and 50 mol% LiFSI concentrations in IL-based electrolytes provides a promising solution for overcoming the limitations of Li–S batteries. These advancements bring Li–S technology closer to practical applications, potentially leading to the development of more efficient and durable energy storage systems for large-scale use. Future research should continue to explore and optimize IL formulations to further enhance the performance and commercial viability of Li–S batteries.

4. Experimental details

4.1. Materials

Trimethyl-iso-butyl phosphonium $P_{111i4}FSI$ ionic liquid was supplied by Solvionic (France), Lithium bis(trifluoromethanesulfonyl)imide (LiTFSI 99.5%) and lithium bis(fluorosulfonyl) imide (LiFSI, 99.5%) were supplied by Nippon Shokubai (Japan). Both materials were used without further purification or drying. All the materials were kept in argon-filled glovebox for further preparation of electrolytes. Sulfur and dehydrated Li_2S powder (99.98%) were purchased from Merck and stored in an argon-filled glovebox.

4.2. Synthesis

Electrolyte composition preparation. The electrolyte solutions are prepared by direct addition of the Li salt (LiFSI or LiTFSI) in the desired concentration to the dried ionic liquid (Schlenk line at 50 °C, 0.6 kPa for 72 h) and dissolved with stirring and heat (24 h at 50 °C). Preparation is performed in an Argon glovebox (O_2 < 0.1 ppm and H_2O < 0.1 ppm), and the ionic liquid and Li salts are further dried on a Schlenk line at 50 °C, 0.6 kPa for 72 h. The obtained clear solutions are stored under argon at RT.

Polysulfide dissolution testing-visual/optical solubility studies. Electrolytes containing 0, 5, 10, 20, 30, 40, 45, and 50 mol% LiTFSI/$[P_{111i4}][FSI]$ solutions were made. The stoichiometric amount of elemental sulfur and Li_2S powder were mixed into the different electrolytes and the solutions were stirred for a long time at 50 °C. The objective of these experiments was to examine polysulfide dissolution in the phosphonium IL electrolytes containing low (≤20 mol% LiTFSI salt) and high concentrations of lithium salt (≥20 mol% LiTFSI salt). Observation of a color change of electrolytes + S + Li_2S solutions would signify the formation and dissolution of any higher-order polysulfides. The dark red color in the neat IL is due to the formation of intermediate polysulfides Li_2S_n ($4 \leq n \leq 8$) which readily dissolve in the neat IL and give it a strong color and readily visually detectable color to the solution. Preparation is performed in an Argon glovebox (O_2 < 0.1 ppm and H_2O < 0.1 ppm).

Sulfur-electrode preparation: 15 wt% CMC, 21 wt% HSAC, 14 wt% C65 and 50 wt% S. Basic electrodes were prepared by making a slurry of high surface area carbon–sulfur composite (30–70 wt% HSAC-S), conductive carbon-C65, and carboxymethyl cellulose (CMC) binder keeping the mass ratio as 70 : 15 : 15, respectively. The solvent used with the CMC binder was deionized water (1 mL DI water/20 mg of CMC binder). The slurry was first cast by using the doctor blade gap of 400 μm on the carbon-coated aluminum current collector and then dried at 80 °C in the oven for 24 h. After drying, the electrode thickness was 110 to 120 μm which reduced to 70 to 80 μm after calendaring using a roll drum calendar (Mediatech). The calendared electrode was utilized for cell making. Further, the electrode is referred to as "15CMC" S-electrode.

4.3. Materials characterizations

Renishaw inVia Visible Raman Microscope, 633 nm laser, power 17 mW, 20× magnification was used to perform the test. UV spectroscopy (UV-2600, SHIMADZU) used to analysis of polysulfides.

4.5. Coin cell assembly and electrochemical measurements

The 15CMC S-electrode was cut into disks of 8 mm diameter, area 0.5 cm^{-2}, the sulfur mass loading on the electrode was 2 mg cm^{-2}. Disks were then used as cathodes to fabricate Li–S cells. To assemble a CR 2032-coin cell, a 15CMC cathode was placed against a 50 μm thin lithium metal foil anode. A polypropylene (Celgard 3501) membrane of 18 mm diameter was incorporated as a separator between the cathode and anode. 45 μL of electrolyte was utilized for each cell. The electrochemical measurements of Li–S cells were carried out at a constant temperature of 50 ± 2 °C in the potential window of 1.5–2.8 V *versus* Li/Li^+ at a current rate of 0.1 C (167 mA g^{-1} sulfur).

4.6. Samples preparation for Raman spectroscopy analysis

Polysulfide solubility in the mixed FSI/TFSI anions electrolytes was examined by Raman spectroscopy which is ultrasensitive for dissolved PS species. Renishaw inVia Visible Raman Microscope, 633 nm laser, power 17 mW, 20× magnification was used to perform the test. The limit of detection of the technique can be increased by using an increasingly higher power laser in the technique. As before, the goal of the sample preparations was to saturate the IL electrolyte with polysulfides. After vigorous mixing at 50 °C, each mixture was centrifuged to separate unreacted sulfur and precipitated Li_2S solid particles from the liquid phase (supernatant) of mixture. The supernatant and dissolved, saturated polysulfide are then transferred to transparent glass narrow capillary tubes for Raman analysis.

Author contributions

The research was conceptualized, and the experiments were developed by A.K., M.F., and P.C.H. A.K. created the framework for the study, carried out the experiments, and wrote the report. A.K., F.N., and J.S. prepared the electrolyte, conducted the dissolution experiments, and helped curate the data. The Raman experiments were carried out by A.K. and M.M. S.R. and Paul M. Bayley supported data analysis and manuscript editing. Throughout the study process, each author contributed significantly and participated actively in discussions. The project was supervised, and the paper was edited by M.F. and P.C.H. All authors reviewed and approved the final version.

Data availability

The data that support the findings of this study are available from the corresponding author upon reasonable request.

Conflicts of interest

The authors declare no conflict of interest.

Acknowledgements

This work is financially supported by the Li–S Energy and REACH funded through the commonwealth government TRAILBLAZER program. This research was undertaken at the Deakin University Battery Research and Innovation Hub (BattRI-Hub), Australia. This work was supported by funding received from the Australian Research Council (ARC) through the ARC Training Centre in Future Energy Storage Technologies IC180100049 (StorEnergy).

References

1 J. J. Marie and S. Gifford, Developments in Lithium-Ion Battery Cathodes, *Faraday Insights*, 2023, (18), 1–12.
2 M. S. Whittingham, Lithium Batteries and Cathode Materials, *Chem. Rev.*, 2004, **104**, 4271–4302.
3 A. Manthiram, Y. Fu, S.-H. Chung, C. Zu and Y.-S. Su, Rechargeable Lithium-Sulfur Batteries, *Chem. Rev.*, 2014, **114**, 11751–11787.
4 Z. W. Seh, Y. Sun, Q. Zhang and Y. Cui, Designing High-Energy Lithium-Sulfur Batteries, *Chem. Soc. Rev.*, 2016, **45**, 5605–5634.
5 S. Evers and L. F. Nazar, New Approaches for High-Energy Density Lithium-Sulfur Battery Cathodes, *Acc. Chem. Res.*, 2013, **46**, 1135–1143, DOI: **10.1021/ar3001348**.
6 X. Ji and L. F. Nazar, Advances in Li-S Batteries, *J. Mater. Chem.*, 2010, **20**, 9821–9826.
7 D. Aurbach, E. Zinigrad, Y. Cohen and H. Teller, A Short Review of Failure Mechanisms of Lithium Metal and Lithiated Graphite Anodes in Liquid Electrolyte Solutions, *Solid State Ionics*, 2002, **148**, 405–416.
8 J. Tan, J. Matz, P. Dong, M. Ye and J. Shen, Appreciating the Role of Polysulfides in Lithium-Sulfur Batteries and Regulation Strategies by Electrolytes Engineering, *Energy Storage Mater.*, 2021, **42**, 645–678.
9 W. Xu, J. Wang, F. Ding, X. Chen, E. Nasybulin, Y. Zhang and J.-G. Zhang, Lithium Metal Anodes for Rechargeable Batteries, *Energy Environ. Sci.*, 2014, **7**, 513–537.
10 Y. Yang, G. Zheng and Y. Cui, Nanostructured Sulfur Cathodes, *Chem. Soc. Rev.*, 2013, **42**, 3018–3032.
11 H. Shin, M. Baek, A. Gupta, K. Char, A. Manthiram and J. W. Choi, Recent Progress in High Donor Electrolytes for Lithium-Sulfur Batteries, *Adv. Energy Mater.*, 2020, **10**, 2001456.
12 Q. Pang, X. Liang, C. Y. Kwok and L. F. Nazar, Advances in Lithium-Sulfur Batteries Based on Multifunctional Cathodes and Electrolytes, *Nat. Energy*, 2016, **1**, 132.
13 G. Di Donato, T. Ates, H. Adenusi, A. Varzi, M. A. Navarra and S. Passerini, Electrolyte Measures to Prevent

Polysulfide Shuttle in Lithium-Sulfur Batteries, *Batteries Supercaps*, 2022, **5**, e202200097.

14 S. S. Zhang, Role of $LiNO_3$ in Rechargeable Lithium/Sulfur Battery, *Electrochim. Acta*, 2012, **70**, 344–348.

15 Laboratory Chemical Safety Summary (LCSS) Datasheet, PubChem CID 10129889, PubChem, **https://pubchem.ncbi.nlm.nih.gov/compound/Lithium-nitrate**.

16 Y. Chen, Y. Kang, Y. Zhao, L. Wang, J. Liu, Y. Li, Z. Liang, X. He, X. Li, N. Tavajohi and B. Li, A Review of Lithium-Ion Battery Safety Concerns: The Issues, Strategies, and Testing Standards, *J. Energy Chem.*, 2021, **59**, 83–99.

17 G. Bieker, J. Wellmann, M. Kolek, K. Jalkanen, M. Winter and P. Bieker, Influence of Cations in Lithium and Magnesium Polysulfide Solutions: Dependence of the Solvent Chemistry, *Phys. Chem. Chem. Phys.*, 2017, **19**, 11152–11162.

18 S. H. Chung and A. Manthiram, Designing Lithium-Sulfur Cells with Practically Necessary Parameters, *Joule*, 2018, **2**, 710–724.

19 J. W. Park, K. Ueno, N. Tachikawa, K. Dokko and M. Watanabe, Ionic Liquid Electrolytes for Lithium-Sulfur Batteries, *J. Phys. Chem. C*, 2013, **117**, 20531–20541.

20 K. Dokko, N. Tachikawa, K. Yamauchi, M. Tsuchiya, A. Yamazaki, E. Takashima, J. W. Park, K. Ueno, S. Seki, N. Serizawa and M. Watanabe, Solvate Ionic Liquid Electrolyte for Li-S Batteries, *J. Electrochem. Soc.*, 2013, **160**, A1304–A1310.

21 K. Ueno, J. W. Park, A. Yamazaki, T. Mandai, N. Tachikawa, K. Dokko and M. Watanabe, Anionic Effects on Solvate Ionic Liquid Electrolytes in Rechargeable Lithium-Sulfur Batteries, *J. Phys. Chem. C*, 2013, **117**, 20509–20516.

22 A. Kilic, O. Abdelaty, M. Zeeshan, A. Uzun, R. Yildirim and D. Eroglu, Selection of Ionic Liquid Electrolytes for High-Performing Lithium-Sulfur Batteries: An Experiment-Guided High-Throughput Machine Learning Analysis, *Chem. Eng. J.*, 2024, **490**, 151562.

23 U. Pal, D. Rakov, B. Lu, B. Sayahpour, F. Chen, B. Roy, D. R. MacFarlane, M. Armand, P. C. Howlett and M. Forsyth, Interphase Control for High Performance Lithium Metal Batteries Using Ether Aided Ionic Liquid Electrolyte, *Energy Environ. Sci.*, 2022, **15**, 1907–1919.

24 U. Pal, G. M. A. Girard, L. A. O'Dell, B. Roy, X. Wang, M. Armand, D. R. MacFarlane, P. C. Howlett and M. Forsyth, Improved Li-Ion Transport by DME Chelation in a Novel Ionic Liquid-Based Hybrid Electrolyte for Li-S Battery Application, *J. Phys. Chem. C*, 2018, **122**, 14373–14382.

25 A. Kumar, A. Ghosh, M. Forsyth, D. R. MacFarlane and S. Mitra, Free-Radical Catalysis and Enhancement of the Redox Kinetics for Room-Temperature Sodium-Sulfur Batteries, *ACS Energy Lett.*, 2020, **5**, 2112–2121.

26 H. L. Wu, L. A. Huff and A. A. Gewirth, In Situ Raman Spectroscopy of Sulfur Speciation in Lithium-Sulfur Batteries, *ACS Appl. Mater. Interfaces*, 2015, **7**, 1709–1719.

27 M. Hagen, P. Schiffels, M. Hammer, S. Dörfler, J. Tübke, M. J. Hoffmann, H. Althues and S. Kaskel, *In situ* Raman Investigation of Polysulfide Formation in Li-S Cells, *J. Electrochem. Soc.*, 2013, **160**, A1205–A1214.

28 G. M. A. Girard, M. Hilder, H. Zhu, D. Nucciarone, K. Whitbread, S. Zavorine, M. Moser, M. Forsyth, D. R. MacFarlane and P. C. Howlett, Electrochemical and Physicochemical Properties of Small Phosphonium Cation Ionic Liquid Electrolytes with High Lithium Salt Content, *Phys. Chem. Chem. Phys.*, 2015, **17**, 8706–8713.